SCIENCE CHINA
Technological Sciences

Special Topic: Chemomechanics
•Article•

August 2019 Vol.62 No.8: 1341–1348
https://doi.org/10.1007/s11431-018-9483-7

A cell-based model for analyzing growth and invasion of tumor spheroids

CHEN PengCheng, LI Bo* & FENG XiQiao*

Institute of Biomechanics and Medical Engineering, AML, Department of Engineering Mechanics, Tsinghua University, Beijing 100084, China

Received December 27, 2018; accepted March 4, 2019; published online July 11, 2019

Both chemical and mechanical determinants adapt and react throughout the process of tumor invasion. In this study, a cell-based model is used to uncover the growth and invasion of a three-dimensional solid tumor confined within normal cells. Each cell is treated as a spheroid that can deform, migrate, and proliferate. Some fundamental aspects of tumor development are considered, including normal tissue constraints, active cellular motility, homotypic and heterotypic intercellular interactions, and pressure-regulated cell division as well. It is found that differential motility between cancerous and normal cells tends to break the spheroidal symmetry, leading to a finger instability at the tumor rim, while stiff normal cells inhibit tumor branching and favor uniform tumor expansion. The heterotypic cell-cell adhesion is revealed to affect the branching geometry. Our results explain many experimental observations, such as fingering invasion during tumor growth, stiffness inhibition of tumor invasion, and facilitation of tumor invasion through cancerous-normal cell adhesion. This study helps understand how cellular events are coordinated in tumor morphogenesis at the tissue level.

tumor, growth, collective invasion, cell-based modeling

Citation: Chen P C, Li B, Feng X Q. A cell-based model for analyzing growth and invasion of tumor spheroids. Sci China Tech Sci, 2019, 62: 1341–1348, https://doi.org/10.1007/s11431-018-9483-7

1 Introduction

Tumorigenesis, i.e., the initiation and development of tumors, is a complicated process which involves not only genetic alterations but also changes in cell migration, cell-cell and cell-matrix interactions and so on [1–3]. To grow in a confined space, an *in vivo* solid tumor has to overcome the geometric constraints of extracellular matrix (ECM) [4,5], which in turn generate compressive stresses in the tumor. Recent experiments revealed that these compressive stresses can inhibit the expansion of a multicellular tumor spheroid (MTS) [6–10]. On the one hand, compressive stresses may lead to cell cycle arrest and even apoptosis [11], which slow down the growth rate of MTS, as experimentally exemplified by tumor growth confined within matrix of different stiffness [7]. On the other hand, compressive stresses applied by ECM or stroma nearby ordinarily lead to differential cell fate from the interior to the periphery of MTS, which causes a stratified structure consisting of a necrotic core, surrounded by a rim of hypermotile and proliferating cells [10].

As a primary tumor grows and undergoes malignant transformation, local invasion may occur, which leads to metastasis to distant organs subsequently [12]. Though various invasion modes have been observed *in vivo*, e.g., single-cell, streaming and collective invasion, mounting evidences indicate that collective invasion dominates in most invasive solid tumors, in which cell-cell connection maintains [13,14]. During collective invasion, intercellular adhesion, cell motility and proliferation are entangled. For example, leader cells with active motility guide the following cells through cell-cell adhesion to invade, wherein uncontrolled

*Corresponding authors (email: libome@tsinghua.edu.cn; fengxq@tsinghua.edu.cn)

cell proliferation renders pushing forces promoting the invasion of cells at the front of the leading edge [3,15]. Notably, tumor invasion involves not only homotypic cell-cell adhesion but also heterotypic adhesion [16–18]. *In vitro* experiments have demonstrated that cancer-associated fibroblast cells or macrophages establish direct communication with cancerous cells through heterotypic E-cadherin/N-cadherin adhesions to facilitate tumor invasion [17,18]. Taken together, tumor growth and invasion involve both mechanical and biological factors, for instance, mechanical stress, stromal stiffness, cell motility and cell-cell adhesion. Though many experiments and *in silico* simulations have been performed [3,15,19–22], it remains elusive how cancerous-cancerous and cancerous-stromal cell interactions, both biological and mechanical, are orchestrated during collective tumor invasion.

To investigate solid tumor growth and invasion, some theoretical models have been developed, which can be divided into continuum [1,19] and discrete models [20–25]. Continuum models often treat a tumor as an elastic/viscoelastic tissue [1], in which field variables are adopted to characterize its growth, deformation, and nutrient transport. In contrast, discrete models including the cellular vertex model [21,22,26,27], the cellular Potts model [20], and the particle model [24,25], are established based on individual cells. However, because of their heavy computational burden at the large scale, the cellular vertex model and the cellular Potts model are limited to population size and usually employed in two-dimensional systems [3,20,22]. Due to its less computational cost, the particle model has been frequently used in three-dimensional (3D) systems, while it treats cells as mass points and ignores some detailed information such as cell deformation, stiffness, and size change. For example, many experiments have shown that during cancerization, cancerous cells are softer than normal cells [28–31] and thus, the stiffness of cancerous cells should be taken into account. To avoid the oversimplification, the cell-based model has also been introduced [24,25,32]. In such a model, cancerous cells are represented by adhesive isotropic elastic spheres capable of deformation, growth and proliferation.

In this paper, we use a cell-based model to investigate the development of a MTS confined in a normal cell aggregate. We focus on how the growth-induced pressure, the elastic moduli of cells, and the intercellular adhesion affect the 3D growth and invasion of a solid tumor. The feedback between pressure and cell division is taken into account. We show that differential cell motility between cancerous cells and normal cells facilitates fingering instability onset at the tumor front. The finger morphology is found to be controlled by normal cell stiffness and heterotypic adhesion strength. The results not only deepen our understanding of many experimental observations on tumor development, but also highlight the role of mechanical factors in tissue morphogenesis.

2 Cell-based model

Consider the growth and invasion of a tumor spheroid within an aggregate of normal cells, mimicking the environmental constraint provided by host tissue *in vivo* (Figure 1(a)) [33]. As observed *in vitro* 3D culture model, individual cells in aggregates cultured in suspension or collagen gels often exhibit a spherical geometry. Here, a cell-based model is adopted to consider the biomechanical interactions between cells during tumor growth and invasion, as shown in Figure 1(b). Each cell is simplified as a deformable sphere. In addition, the mechanism of pressure-regulated cell division rule is incorporated (Figure 1(c)) [24,25,34]. Langevin dynamic theory is invoked to govern cell motion, where inertia is neglected while damping effect dominates [35]. Considering intercellular interactions and force equilibrium of cells, the equation of motion of type X cell i is described as

$$\gamma^{\mathrm{XM}}\frac{\mathrm{d}\mathbf{r}_i^{\mathrm{X}}}{\mathrm{d}t}=\sum_{j\in\mathrm{NX}}\left(\gamma^{\mathrm{XX}}\left(\mathbf{v}_j^{\mathrm{X}}-\mathbf{v}_i^{\mathrm{X}}\right)\cdot\mathbf{n}^{\mathrm{XX}}\mathbf{n}^{\mathrm{XX}}+\mathbf{F}_{ij}^{\mathrm{XX}}\right)+\mathbf{F}_i^{\mathrm{XA}}+\sum_{j\in\mathrm{NY}}\left(\gamma^{\mathrm{XY}}\left(\mathbf{v}_j^{\mathrm{Y}}-\mathbf{v}_i^{\mathrm{X}}\right)\cdot\mathbf{n}^{\mathrm{YX}}\mathbf{n}^{\mathrm{YX}}+\mathbf{F}_{ij}^{\mathrm{YX}}\right),\tag{1}$$

where the superscripts $\mathrm{X},\mathrm{Y}\in\{\mathrm{N},\mathrm{C}\}$ and $\mathrm{X}\neq\mathrm{Y}$. C and N indicate cancerous and normal cells, respectively; γ^{XM} denotes damping coefficient of migrating type X cells in surrounding matrix; γ^{XX} and γ^{XY} represent the friction coefficients between homotypic cells and heterotypic cells, respectively. The first terms within the two summation symbols account for the friction between cells, with $\mathbf{n}^{\mathrm{XX}}=\left(\mathbf{r}_j^{\mathrm{X}}-\mathbf{r}_i^{\mathrm{X}}\right)/\left|\mathbf{r}_j^{\mathrm{X}}-\mathbf{r}_i^{\mathrm{X}}\right|$ and $\mathbf{n}^{\mathrm{YX}}=\left(\mathbf{r}_j^{\mathrm{Y}}-\mathbf{r}_i^{\mathrm{X}}\right)/\left|\mathbf{r}_j^{\mathrm{Y}}-\mathbf{r}_i^{\mathrm{X}}\right|$. $\mathbf{F}_{ij}^{\mathrm{XX}}$ and $\mathbf{F}_{ij}^{\mathrm{YX}}$ characterize the interaction forces between cells. Summation is taken over all neighboring cells. $\mathbf{F}_i^{\mathrm{XA}}$ is active force of type X cells. All these forces will be detailed below.

2.1 Interactions between contacting cells

Experiments revealed that interactions between contacting cells can be classified into two main types. One is adhesive force arising from membrane proteins such as E-cadherin and another is repelling force stemming from cortical tension or resistance to deformation of cytoskeleton [36,37]. To capture this feature, the Johnson-Kendall-Roberts (JKR) model is introduced to characterize the interactions between spherical cells [38]. The JKR force acting on cell i, which arises from its contacting with neighboring cell j, can be expressed as

$$\mathbf{F}_{ij}^{\mathrm{XY}}=F_{ij}^{\mathrm{XY}}\frac{\mathbf{r}_i^{\mathrm{X}}-\mathbf{r}_j^{\mathrm{Y}}}{\left|\mathbf{r}_i^{\mathrm{X}}-\mathbf{r}_j^{\mathrm{Y}}\right|},\tag{2}$$

where F_{ij}^{XY} is the magnitude of the JKR force between cell i and cell j. It satisfies [25]

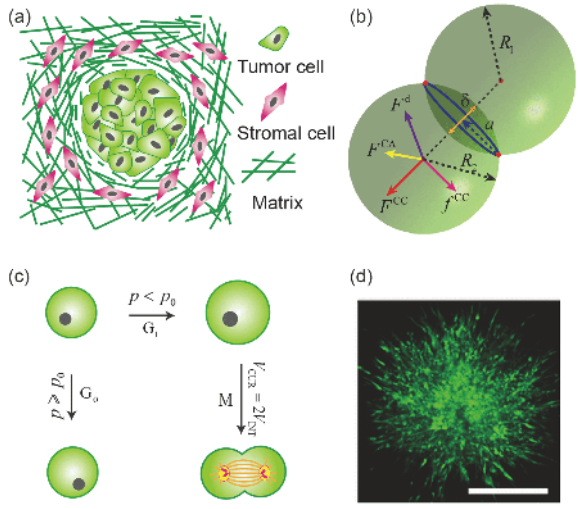

Figure 1 (Color online) (a) A tumor spheroid growing under environmental constraint. (b) Forces applied on interacting cells. (c) Illustration of pressure-regulated cell growth and division rule. During cell proliferation, cell will enter G1 phase and cell volume will increase at a constant rate to realize duplication. While cells undergoing strong compression will stop duplication and are arrested in G0 phase. After G1 phase and cell volume reaches a threshold, mother cell will enter M phase and divide into two daughter cells. (d) Experimental observation of fingering invasion of a MDA-MB-231 cell aggregate embedded in gels. Reprinted from ref. [33] with permission. Scale bar = 500 μm.

$$\delta_{ij}^{\mathrm{XY}}=\frac{\left(a_{ij}^{\mathrm{XY}}\right)^2}{\overline{R}_{ij}^{\mathrm{XY}}}-\sqrt{\frac{2\pi\hat{\gamma}^{\mathrm{XY}}a_{ij}^{\mathrm{XY}}}{\overline{E}_{ij}^{\mathrm{XY}}}},$$
$$\left(a_{ij}^{\mathrm{XY}}\right)^3=\frac{3\overline{R}_{ij}^{\mathrm{XY}}}{4\overline{E}_{ij}^{\mathrm{XY}}}\left[F_{ij}^{\mathrm{XY}}+3\pi\hat{\gamma}^{\mathrm{XY}}\overline{R}_{ij}^{\mathrm{XY}}+\sqrt{6\pi\hat{\gamma}^{\mathrm{XY}}\overline{R}_{ij}^{\mathrm{XY}}F_{ij}^{\mathrm{XY}}+\left(3\pi\hat{\gamma}^{\mathrm{XY}}\overline{R}_{ij}^{\mathrm{XY}}\right)^2}\right], \tag{3}$$

where $\overline{R}_{ij}^{\mathrm{XY}}$ and $\overline{E}_{ij}^{\mathrm{XY}}$ are the equivalent radius and elastic modulus defined by $1/\overline{R}_{ij}^{\mathrm{XY}}=1/R_i^{\mathrm{X}}+1/R_j^{\mathrm{Y}}$ and $1/\overline{E}_{ij}^{\mathrm{XY}}=\left[1-\left(\nu_i^{\mathrm{X}}\right)^2\right]/E_i^{\mathrm{X}}+\left[1-\left(\nu_j^{\mathrm{Y}}\right)^2\right]/E_j^{\mathrm{Y}}$, respectively. R_i^{X}, E_i^{X} and ν_i^{X} denote radius, elastic modulus and the Poisson's ratio of cell i respectively. $\delta_{ij}^{\mathrm{XY}}$ is the sum of displacement due to deformation along the line linking centers of two contacting cells and a_{ij}^{XY} is the radius of the contacting region (Figure 1(b)). $\hat{\gamma}^{\mathrm{XY}}$ denotes the adhesive surface energy between contacting cells. Replacing Y by X, $\mathbf{F}_{ij}^{\mathrm{XX}}$ is defined in a similar way.

2.2 Active force

We consider isotropic micro-motility of cells, instead of biased cell migration such as chemotaxis or durotaxis. In this situation, active forces can be modeled by random fluctuations. We assume that active forces satisfy $\left\langle\mathbf{F}_i^{\mathrm{XA}}\right\rangle=0$ and $\left\langle\mathbf{F}_i^{\mathrm{XA}}(t_1),\mathbf{F}_i^{\mathrm{XA}}(t_2)\right\rangle=6(\gamma^{\mathrm{XM}})^2D^{\mathrm{X}}\delta(t_1-t_2)$, in analogy of the passive impact of fluid molecules on Brownian particles [25].

2.3 Cell growth and division

Experimental evidence has demonstrated that compressive force may suppress cell division [39]. However, how cells sense and respond to compressive stresses is still poorly known, which makes it difficult to quantitatively characterize the contribution of stress on cell growth and division. In the present study, we assume cancerous cell growth and division are regulated by total pressure. Because it is hard to exactly evaluate the total pressure applied on a cell in the discrete model, we follow the previous studies [25,40] to calculate the total pressure as the summation of the normal pressure exerted on cells. Therefore, the calculated total pressure is different from the definition of hydrostatic pressure. For simplicity, only G_1, M and G_0 phases are considered [34]. The total pressure p_i^{C} is defined by [25]

$$p_i^{\mathrm{C}}=\sum_{j\in\mathrm{NC}}\left(\frac{\mathbf{F}_{ij}^{\mathrm{CC}}}{A_{ij}^{\mathrm{CC}}}\cdot\frac{\mathbf{r}_i^{\mathrm{C}}-\mathbf{r}_j^{\mathrm{C}}}{\left|\mathbf{r}_i^{\mathrm{C}}-\mathbf{r}_j^{\mathrm{C}}\right|}\right)+\sum_{j\in\mathrm{NN}}\left(\frac{\mathbf{F}_{ij}^{\mathrm{NC}}}{A_{ij}^{\mathrm{NC}}}\cdot\frac{\mathbf{r}_i^{\mathrm{C}}-\mathbf{r}_j^{\mathrm{N}}}{\left|\mathbf{r}_i^{\mathrm{C}}-\mathbf{r}_j^{\mathrm{N}}\right|}\right), \tag{4}$$

where A_{ij}^{CC} and A_{ij}^{NC} denote the area of contacting regions between cells. If the pressure p_i^{C} exerted on cancerous cell i satisfies $p_i^{\mathrm{C}}<p_0$, with p_0 being the pressure threshold, the cell will enter G_1 phase and its radius will enlarge at a constant rate v_g; while cell growth will stop when p_i^{C} exceeds p_0, which means cell growth is arrested in G_0 phase [39].

We assume that cells enter M phase and division begins immediately after the end checkpoint of G_1 phase, where the current cell volume is twice the initial cell volume, that is, $V_{\mathrm{CUR}}=2V_{\mathrm{INT}}$. Though cells deform during growth process, the volume of cell i is approximated by $V_i=4\pi R_i^3/3$. After volume doubles, cells divide into two dumb-bell shaped daughter cells, which are placed at a given separation distance. The orientation of cell division is randomly chosen. Cell apoptosis is not considered in the present study. Though some cells are arrested in G_0 phase, they can still recover to growth and divide when the total pressure exerted on them is smaller than p_0.

3 Model setup and computation

Initially, we consider a cancerous cell embedded in an environmental normal cell population. It may grow and expand to form a multicellular tumor spheroid. The normal cells with fixed population distribute uniformly in a space confined by

a spherical boundary at the initial state. The diameter of the confined space is 500 μm and the density of normal cells is set as $\rho^{N} = 2 \times 10^{5} / \mathrm{mm}^{3}$ [25]. The boundary is described by a spherical lumen, which interacts with cells and generates forces to prevent cells from penetrating and escaping. JKR force is also employed to characterize the interaction between cells and boundary. Migration of cancerous and normal cells is governed by the motion eq. (1). We take the centroid of the spherical lumen as the origin, with r denoting the radial distance deviating from the origin.

To normalize the system, we chose the following basic parameters: the diameter of cells $L = 2R$=15 μm, the cell cycle τ=18 h, and the reference energy $F_{T} = 10^{-16}$ J [24,25]. The system is rescaled by the length scale L, the time scale τ, and the force scale F_{T}/L. Introduce two significant dimensionless parameters: $\alpha=\gamma^{NM}/\gamma^{CM}$ characterizing differential motility between cancerous cells and normal cells and $\beta=\tilde{\gamma}^{CN}/\tilde{\gamma}^{CC}$ characterizing relative strength between cancerous-normal and cancerous-cancerous cell adhesion. Table 1 shows the model parameters and their typical values used in the simulations. The simulations are implemented by the explicit Euler method with a time step of 0.001. Generally, $\sim 2 \times 10^{4}$ steps are calculated for the system to evolve. All calculations are performed in MATLAB.

4 Results and discussion

4.1 Pressure distribution

Experimental observations have confirmed that compressive stresses arising from surrounding cells or host tissue confinements can inhibit cell proliferation during tumor growth [7–9,46,47]. To capture this feature, a pressure-regulated proliferation rule has been introduced at the cellular scale in our model. We next examine the pressure field at the tissue level.

Firstly, our model can recapitulate the formation of a multicellular tumor spheroid under confinement, as shown in Figure 2(a). We further plot the pressure distribution inside a tumor spheroid in Figure 2(b). Two different regions of pressure distribution are observed. In the central region of tumor spheroid, pressure is high, where most cells are arrested and cell division is suppressed. At the periphery of tumor spheroid, pressure is low and even stretching occurs, where cells proliferate normally, in agreement with the stratified structure observed *in vitro* experiments [10]. To quantify pressure distribution, averaged pressure along radial direction is shown in Figure 2(c), where decreasing pressure from the interior to the periphery of tumor spheroid is remarkable. To reflect the local crowdedness of cancerous cells, a packing fraction is introduced. The packing fraction is defined as $\Phi = \sum_{c \in \Lambda} V_{c}/V_{s}$, where Λ denotes a subregion and V_{c}/V_{s} means the ratio between the total volume of cells in the subregion Λ and the volume of the subregion itself [48]. Clearly, cancerous cells are more crowded, when they are closer to the center of the tumor spheroid, indicating a strong correlation between pressure and cell crowding (Figure 2(c)).

4.2 Finger formation

After initial uniform expansion, local tumor invasion and metastasis may happen. Various invasive behaviors of cancerous cells have been observed *in vitro* experiments [49]. Fingering is a typical mode of tumor invasion, which was found when a MTS was embedded in 3D collagen gels, as

Table 1 Model parameters

Parameter	Symbol	Unit	Value	Source
Young's modulus of cells	E^{C}, E^{N}	Pa	450, 1000	[41]
Poisson's ratio of cells	ν^{C}, ν^{N}	–	0.4	[42]
Adhesive energy between cells	$\tilde{\gamma}^{CC}, \tilde{\gamma}^{NN}$	J/m^2	10^{-4}	[43]
Reference diffusion constant	D_0	cm^2 s^{-1}	10^{-12}	[44]
Diffusion constant of cells	D^{C}, D^{N}	cm^2 s^{-1}	10^{-12}	Assumed
Reference friction coefficient	γ_0	N s/m	1	[44]
Friction coefficient between cells	$\gamma^{CN}, \gamma^{CC}, \gamma^{NN}$	N s/m	1, 0.02, 0.02	Assumed
Radius of cells	R	μm	7.5	[25]
Cell cycle	τ	h	18	[45]
Pressure threshold	p_0	Pa	100–450	Assumed
Radius of environment	R_{EN}	μm	250	[7]
Growth rate of radius	v_g	μm/h	0.1083	Assumed
Time step	Δt	τ	0.001	–

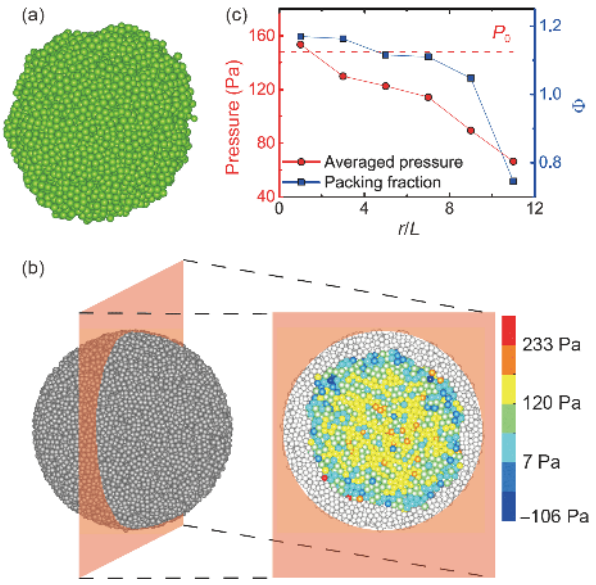

Figure 2 (Color online) (a) Formation of a multicellular tumor spheroid. (b) Snapshot of pressure distribution inside a tumor spheroid at t=14τ. Light grey particles denote normal cells, otherwise cancerous cells. (c) Averaged pressure and packing fraction Φ as a function of radial distance r deviating from the centroid of the fixed spherical lumen. In all simulations, we take α=1, p_0=148 Pa, and E^{N}=1000 Pa.

shown in Figure 1(d) [33,50,51].

Our simulations show that when cancerous cells have the same motility as normal ones, i.e., α=1, tumor spheroid tends to maintain a nearly spherical shape during expansion and no obvious invasion is observed (Figure 3(a)). However, if motility of cancerous cells is stronger than that of normal ones, e.g., α=5, tumor spheroid will lose its smooth periphery, where slight perturbation of spherical boundary appears (Figure 3(b)). Further enlarging differential motility between cancerous and normal cells, e.g., α=20 and 50, tumor spheroid protrudes more fingers and cell mixing happens at the boundary of tumor spheroid, as shown in Figure 3(c) and (d). These results indicate that stronger motility of cancerous cells than that of normal cells is apt to drive tumor invasion toward the host tissue.

To characterize tumor growth, we calculate cancerous cell number N^{C} and the gyration radius

$$R_g = \sqrt{\sum_i^{N^{\mathrm{C}}} (\mathbf{r}_i - \mathbf{R}_{\mathrm{CM}})^2 / N^{\mathrm{C}}},$$

where $\mathbf{R}_{\mathrm{CM}} = \sum_i^{N^{\mathrm{C}}} \mathbf{r}_i / N^{\mathrm{C}}$ [25]. It is found that the size of cancerous cell population enlarges at a slower rate with a higher motility α (Figure 4(a)). In addition, linear growth of the radius of gyration emerges at a long time scale and the growth rate is reduced by increasing α, as shown in Figure 4(b).

The invasion degree of cancerous-normal cell system can be quantified by

$$\rho(t) = \left\langle \frac{n^i_{\mathrm{hetero}}}{n^i_{\mathrm{hetero}} + n^i_{\mathrm{homo}}} \right\rangle_i, \quad (5)$$

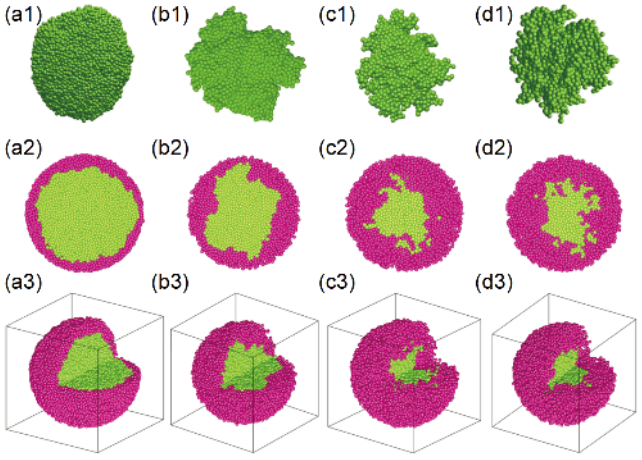

Figure 3 (Color online) Snapshots of fingering invasion during tumor growth. (a1)–(d1) Morphology of tumor spheroids. (a2)–(d2) Hemispherical cross-section of tumor invasion. (a3)–(d3) 3D view with a quarter of space removed. (a) α=1, t=14τ; (b) α=5, t=14τ; (c) α=20, t=14τ; (d) α=50, t=16τ. Red and green spheres denote normal cells and cancerous cells, respectively. In all simulations, we take p_0=444 Pa and E^{N} = 1000 Pa.

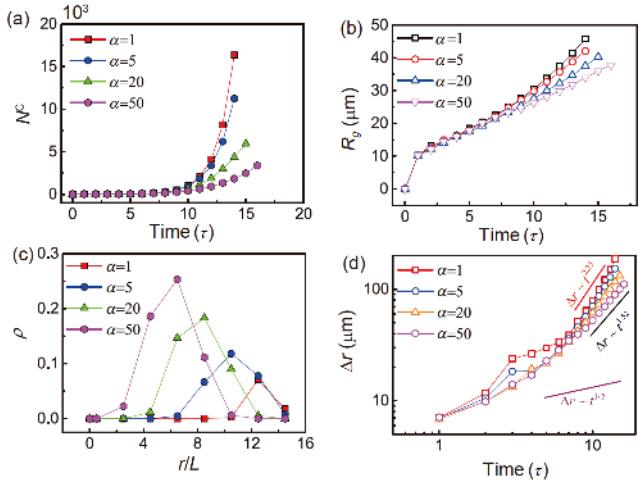

Figure 4 (Color online) Simulation results under different α. (a) Cancerous cell number N^{C} versus time; (b) the radius of gyration of tumor spheroid R_g; (c) dependence of invasion degree ρ on the radial distance r at t=14τ; (d) invasion distance Δr as a function of time.

where n^i_{hetero} is the heterotypic neighbors of cell i (i.e., cancerous-normal pairs) and n^i_{homo} denotes the homotypic neighbors of cell i (i.e., cancerous-cancerous pairs or normal-normal pairs) [3]. $\langle\cdot\rangle_i$ means average over all cells. The invasion distance Δr is calculated by $\Delta r(t) = \sum_i^{N_{\mathrm{b}}} |\mathbf{r}_i - \mathbf{R}_{\mathrm{CM}}| / N_{\mathrm{b}}$, where N_{b} is the number of cancerous cells at the boundary [40]. Our results reveal that the invasion degree ρ is a unimodal function of radial distance r. At the central region of the spheroid that is occupied by cancerous cells entirely, ρ vanishes. ρ peaks at the middle region, indicating mixing of cancerous and normal cells

occurs there, and reduces to 0 at the periphery occupied by only normal cells (Figure 4(c)). Therefore, the width of the peak can be employed to describe the length of the invasion finger. It can be seen that the tumor spheroid is more aggressive and longer protrusion fingers emerge under a higher α. Previous results showed that the invasion distance Δr increases as a function of time at a rate of $\Delta r \sim t^{1/2}$, which results from persistent random walking of invading cells in the spheroid [52]. Here, we find that a higher exponent is observed at a long time scale, which implies super diffusion of invading cancerous cells happens in our system, as shown in Figure 4(d) [25,40].

4.3 Effect of stiffness of normal cells

Experiments for LS174T spheroids showed that the growth rate of a tumor spheroid embedded in stiffer gels is slower [7]. It suggests that stiffness of microenvironment plays a key role in tumor growth. We next examine how stiffness of normal cells influences tumor invasion.

As shown in Figure 5(a), when normal cells are softer than cancerous cells (E^{C}=450 Pa), e.g., E^{N}=300 Pa, invasive fingers appear evidently, indicating a highly invasive behavior. While for the case, where normal cells are stiffer than cancerous cells, a situation observed in most solid tumors [28], e.g., E^{N}=600 Pa or E^{N}=2000 Pa, tumor invasion tends to be suppressed. In this situation, brunching morphology is not evident and a relatively smooth boundary is observed (Figure 5(b) and (c)).We further measure the cancerous cell population size N^{C}, the radius of gyration R_g and the invasion degree ρ. Our quantitative results show that stiffer normal cells inhibit tumor growth, as shown in Figure 5(d) and (e), in agreement with experimental observations [7]. In addition, the elasticity of normal cells significantly affects tumor invasion as well. With increasing stiffness of normal cells, the invasion degree of tumor spheroid declines, as shown in Figure 5(f). Of note, some *in vitro* cancerous cells cultured on two-dimensional (2D) elastic gels may exhibit opposite behavior. For example, *in vitro* 2D experiments found that cancerous cells display rigidity-dependent proliferation or migration, such as enhanced proliferation rate and motility of glioma cells with increasing substrate rigidity [53]. In addition, increased substrate rigidity was found to promote invadopodia activity and drive an invasive phenotype [54,55]. These results clearly show that tumor growth in 3D assays, where cells sense pressure or stresses from all directions, bears profoundly distinct features compared with 2D cases.

4.4 Effects of cancerous-normal cell adhesion

Increasing experimental observations revealed that several stromal cells may cooperate with tumor cells and facilitate tumor invasion, such as cancer associated fibroblast cells and macrophages [17,18]. We next examine how cancerous-normal cell interaction contributes to tumor invasion. Motivated by experimental observation that heterotypic adhesion between cancerous and normal cells drives tumor invasion [17], we focus on the effect of abnormal adhesion established between cancerous and normal cells.

Compared with Figure 3(b2), heterotypic adhesion endows tumor spheroid highly aggressive phenotype, as shown in Figure 6(a)–(c). With increasing cancerous-normal adhesion

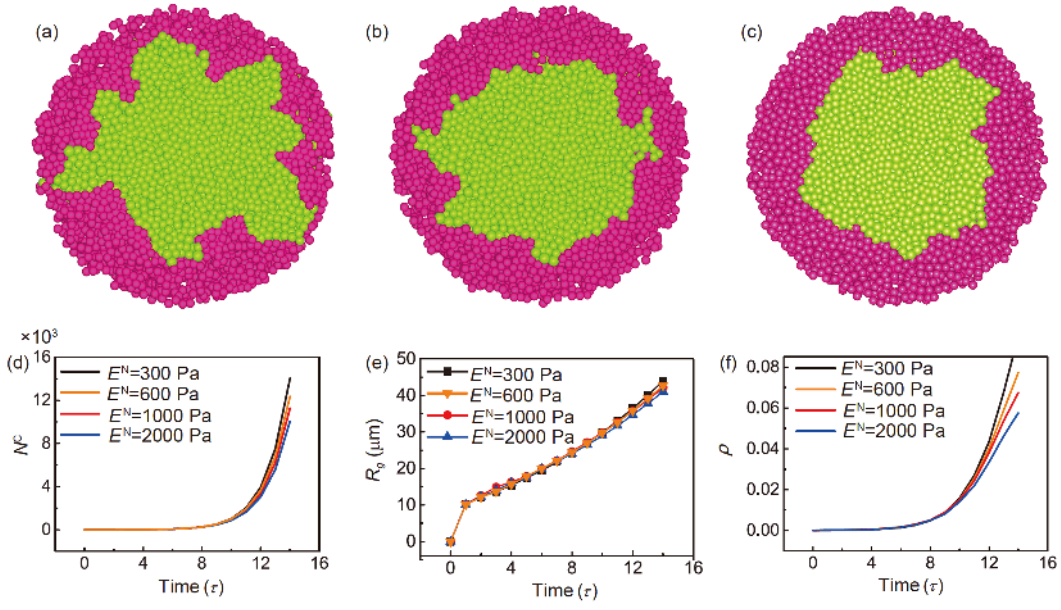

Figure 5 (Color online) Impact of stiffness of normal cells on tumor growth. (a) E^{N}=300 Pa; (b) E^{N}=600 Pa; (c) E^{N}=2000 Pa. Snapshot at t=14τ. Red and green spheres denote normal cells and cancerous cells respectively. (d) Cancerous cell number N^{C} versus time. (e) The radius of gyration of tumor spheroid R_g. (f) Invasion degree ρ as a function of time. In all simulations, we take α=5 and p_0=444 Pa.

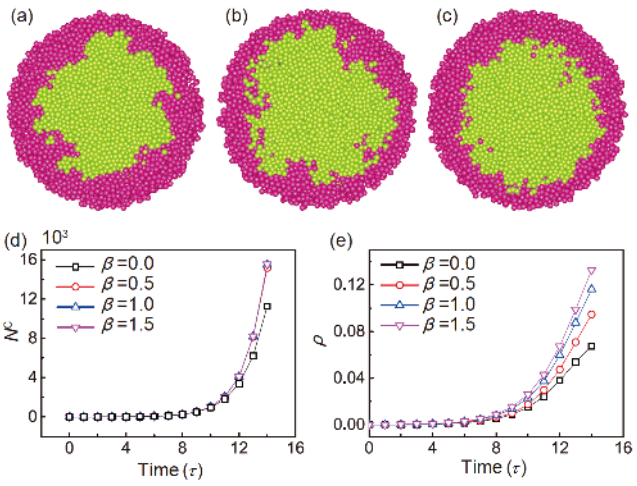

Figure 6 (Color online) Impact of heterotypic adhesion between normal cells and cancerous cells on tumor invasion under different β. (a) β=0.5; (b) β=1; (c) β=1.5. Snapshot at t=14τ. (d) Cancerous cell population size increases as a function of time. (e) Invasion degree versus time. In all simulations, we take α=5, p_0=444 Pa and E^N=1000 Pa.

strength, i.e. β, a sparse and diffusive boundary, instead of a clear boundary, is observed. In addition, cell mixing not only happens at the boundary, but also appears in the interior of tumor spheroid. To characterize the impact of heterotypic adhesion on tumor growth and invasion, the cancerous cell population size and the invasion degree are calculated. It reveals that the strength of adhesion influences tumor growth slightly (Figure 6(d)). However, the invasion degree ρ is sensitive to the increasing strength of cancerous-normal cell adhesion (Figure 6(e)), which explains the branching morphology shown in Figure 6(a)–(c) quantitatively.

5 Conclusions

A cell-based model has been employed to simulate growth and invasion of tumor spheroid confined in normal tissue cells. Mechanical interactions between cells and pressure-regulated cell division are incorporated. Our results reveal that differential motility between cancerous and normal cells regulates fingering invasion of the tumor spheroid. In addition, the elasticity of normal cells and the heterotypic adhesion strength between cancerous and normal cells are shown to significantly affect invasion morphology, and cell proliferation as well. This study helps understand the role of mechanical interactions in tumor growth and invasion.

This work suggests that besides cancerous cell, the mechanical properties of tumor microenvironment and paracancerous normal cells should be inspected in cancer diagnosis and treatment in clinics. It also inspires combinatorial strategies of cancer medicines that target both cancerous and paracancerous cells to control tumor progression.

This work was supported by the National Natural Science Foundation of China (Grant Nos. 11672161, 11620101001).

1 Xue S L, Li B, Feng X Q, et al. Biochemomechanical poroelastic theory of avascular tumor growth. J Mech Phys Solids, 2016, 94: 409–432
2 Tracqui P. Biophysical models of tumour growth. Rep Prog Phys, 2009, 72: 056701
3 Lin S Z, Li B, Xu G K, et al. Collective dynamics of cancer cells confined in a confluent monolayer of normal cells. J Biomech, 2017, 52: 140–147
4 Lu P, Weaver V M, Werb Z. The extracellular matrix: A dynamic niche in cancer progression. J Cell Biol, 2012, 196: 395–406
5 Frantz C, Stewart K M, Weaver V M. The extracellular matrix at a glance. J Cell Sci, 2010, 123: 4195–4200
6 Delarue M, Montel F, Vignjevic D, et al. Compressive stress inhibits proliferation in tumor spheroids through a volume limitation. Biophys J, 2014, 107: 1821–1828
7 Helmlinger G, Netti P A, Lichtenbeld H C, et al. Solid stress inhibits the growth of multicellular tumor spheroids. Nat Biotechnol, 1997, 15: 778–783
8 Montel F, Delarue M, Elgeti J, et al. Isotropic stress reduces cell proliferation in tumor spheroids. New J Phys, 2012, 14: 055008
9 Montel F, Delarue M, Elgeti J, et al. Stress clamp experiments on multicellular tumor spheroids. Phys Rev Lett, 2011, 107: 188102
10 Alessandri K, Sarangi B R, Gurchenkov V V, et al. Cellular capsules as a tool for multicellular spheroid production and for investigating the mechanics of tumor progression *in vitro*. Proc Natl Acad Sci USA, 2013, 110: 14843–14848
11 Levayer R, Dupont C, Moreno E. Tissue crowding induces caspase-dependent competition for space. Curr Biol, 2016, 26: 670–677
12 Fidler I J. The pathogenesis of cancer metastasis: The "seed and soil" hypothesis revisited. Nat Rev Cancer, 2003, 3: 453–458
13 Haeger A, Krause M, Wolf K, et al. Cell jamming: Collective invasion of mesenchymal tumor cells imposed by tissue confinement. Biochim Biophysica Acta (BBA)-General Subjects, 2014, 1840: 2386–2395
14 Friedl P, Locker J, Sahai E, et al. Classifying collective cancer cell invasion. Nat Cell Biol, 2012, 14: 777–783
15 Turner S, Sherratt J A. Intercellular adhesion and cancer invasion: A discrete simulation using the extended Potts model. J Theor Biol, 2002, 216: 85–100
16 Hanahan D, Coussens L M. Accessories to the crime: Functions of cells recruited to the tumor microenvironment. Cancer Cell, 2012, 21: 309–322
17 Labernadie A, Kato T, Brugués A, et al. A mechanically active heterotypic E-cadherin/N-cadherin adhesion enables fibroblasts to drive cancer cell invasion. Nat Cell Biol, 2017, 19: 224–237
18 Condeelis J, Pollard J W. Macrophages: Obligate partners for tumor cell migration, invasion, and metastasis. Cell, 2006, 124: 263–266
19 Roose T, Chapman S J, Maini P K. Mathematical models of avascular tumor growth. SIAM Rev, 2007, 49: 179–208
20 Szabó A, Merks R M H. Cellular potts modeling of tumor growth, tumor invasion, and tumor evolution. Front Oncol, 2013, 3: 87
21 Lin S Z, Li B, Feng X Q. A dynamic cellular vertex model of growing epithelial tissues. Acta Mech Sin, 2017, 33: 250–259
22 Li B, Sun S X. Coherent motions in confluent cell monolayer sheets. Biophys J, 2014, 107: 1532–1541
23 Honda H, Tanemura M, Nagai T. A three-dimensional vertex dynamics cell model of space-filling polyhedra simulating cell behavior in a cell aggregate. J Theor Biol, 2004, 226: 439–453
24 Drasdo D, Höhme S. A single-cell-based model of tumor growth *in vitro*: Monolayers and spheroids. Phys Biol, 2005, 2: 133–147
25 Drasdo D, Hoehme S. Modeling the impact of granular embedding media, and pulling versus pushing cells on growing cell clones. New J Phys, 2012, 14: 055025
26 Lin S Z, Li B, Lan G, et al. Activation and synchronization of the

oscillatory morphodynamics in multicellular monolayer. Proc Natl Acad Sci USA, 2017, 114: 8157–8162
27 Lin S Z, Xue S L, Li B, et al. An oscillating dynamic model of collective cells in a monolayer. J Mech Phys Solids, 2018, 112: 650–666
28 Cross S E, Jin Y S, Rao J, et al. Nanomechanical analysis of cells from cancer patients. Nat Nanotech, 2007, 2: 780–783
29 Hou H W, Li Q S, Lee G Y H, et al. Deformability study of breast cancer cells using microfluidics. Biomed Microdevices, 2009, 11: 557–564
30 Lee G Y H, Lim C T. Biomechanics approaches to studying human diseases. Trends Biotech, 2007, 25: 111–118
31 Li Q S, Lee G Y H, Ong C N, et al. AFM indentation study of breast cancer cells. Biochem Biophys Res Commun, 2008, 374: 609–613
32 Chen P C, Lin S Z, Xu G K, et al. Three-dimensional collective cell motions in an acinus-like lumen. J Biomech, 2019, 84: 234–242
33 Carey S P, Starchenko A, McGregor A L, et al. Leading malignant cells initiate collective epithelial cell invasion in a three-dimensional heterotypic tumor spheroid model. Clin Exp Metastasis, 2013, 30: 615–630
34 Schaller G, Meyer-Hermann M. Multicellular tumor spheroid in an off-lattice Voronoi-Delaunay cell model. Phys Rev E, 2005, 71: 051910
35 Ladoux B, Mège R M. Mechanobiology of collective cell behaviours. Nat Rev Mol Cell Biol, 2017, 18: 743–757
36 Frixen U H. E-cadherin-mediated cell-cell adhesion prevents invasiveness of human carcinoma cells. J Cell Biol, 1991, 113: 173–185
37 Smith P G, Deng L, Fredberg J J, et al. Mechanical strain increases cell stiffness through cytoskeletal filament reorganization. Am J Physiol-Lung Cellular Mol Physiol, 2003, 285: L456–L463
38 Johnson K L, Kendall K, Roberts A D. Surface energy and the contact of elastic solids. Proc R Soc A-Math Phys Eng Sci, 1971, 324: 301–313
39 Li K W, Falcovitz Y H, Nagrampa J P, et al. Mechanical compression modulates proliferation of transplanted chondrocytes. J Orthop Res, 2000, 18: 374–382
40 Malmi-Kakkada A N, Li X, Samanta H S, et al. Cell growth rate dictates the onset of glass to fluidlike transition and long time superdiffusion in an evolving cell colony. Phys Rev X, 2018, 8: 021025
41 Davidson L A, Koehl M, Keller R, et al. How do sea urchins invaginate? Using biomechanics to distinguish between mechanisms of primary invagination. Development, 1995, 121: 2005–2018
42 Mahaffy R E, Shih C K, MacKintosh F C, et al. Scanning probe-based frequency-dependent microrheology of polymer gels and biological cells. Phys Rev Lett, 2000, 85: 880–883
43 Chesla S E, Selvaraj P, Zhu C. Measuring two-dimensional receptor-ligand binding kinetics by micropipette. Biophys J, 1998, 75: 1553–1572
44 Beysens D A, Forgacs G, Glazier J A. Cell sorting is analogous to phase ordering in fluids. Proc Natl Acad Sci USA, 2000, 97: 9467–9471
45 Vintermyr O K, Døskeland S O. Cell cycle parameters of adult rat hepatocytes in a defined medium. A note on the timing of nucleolar DNA replication. J Cell Physiol, 1987, 132: 12–21
46 Cheng G, Tse J, Jain R K, et al. Micro-environmental mechanical stress controls tumor spheroid size and morphology by suppressing proliferation and inducing apoptosis in cancer cells. PLoS ONE, 2009, 4: e4632
47 Ambrosi D, Preziosi L, Vitale G. The interplay between stress and growth in solid tumors. Mech Res Commun, 2012, 42: 87–91
48 Durian D J. Bubble-scale model of foam mechanics: Melting, nonlinear behavior, and avalanches. Phys Rev E, 1997, 55: 1739–1751
49 Yilmaz M, Christofori G, Lehembre F. Distinct mechanisms of tumor invasion and metastasis. Trends Mol Med, 2007, 13: 535–541
50 Kaufman L J, Brangwynne C P, Kasza K E, et al. Glioma expansion in collagen I matrices: Analyzing collagen concentration-dependent growth and motility patterns. Biophys J, 2005, 89: 635–650
51 Ahmadzadeh H, Webster M R, Behera R, et al. Modeling the two-way feedback between contractility and matrix realignment reveals a nonlinear mode of cancer cell invasion. Proc Natl Acad Sci USA, 2017, 114: E1617–E1626
52 Jimenez Valencia A M, Wu P H, Yogurtcu O N, et al. Collective cancer cell invasion induced by coordinated contractile stresses. Oncotarget, 2015, 6: 43438–43451
53 Ulrich T A, de Juan Pardo E M, Kumar S. The mechanical rigidity of the extracellular matrix regulates the structure, motility, and proliferation of glioma cells. Cancer Res, 2009, 69: 4167–4174
54 Alexander N R, Branch K M, Parekh A, et al. Extracellular matrix rigidity promotes invadopodia activity. Curr Biol, 2008, 18: 1295–1299
55 Parekh A, Ruppender N S, Branch K M, et al. Sensing and modulation of invadopodia across a wide range of rigidities. Biophys J, 2011, 100: 573–582